

$-d(\ln j)/d(\ln E)$ implied by corotation and the values measured directly by multi-channel detectors of the Goddard Space Flight Center group (19, 20).

Conclusions. In the interest of brevity, the various conclusions of the previous sections are not repeated here but an overview of them is given in the abstract.

J. A. VAN ALLEN, M. F. THOMSEN
B. A. RANDALL, R. L. RAIDEN
C. L. GROSSKREUTZ

Department of Physics and Astronomy,
University of Iowa,
Iowa City 52242

References and Notes

1. J. W. Dyer, *Science* **207**, 400 (1980).
2. L. W. Brown, *Astrophys. J.* **198**, L89 (1975).
3. M. L. Kaiser and R. G. Stone, *Science* **189**, 285 (1975).
4. J. A. Van Allen, D. N. Baker, B. A. Randall, D. D. Sentman, *J. Geophys. Res.* **79**, 3559 (1974).
5. J. A. Van Allen, B. A. Randall, D. N. Baker, C. K. Goertz, D. D. Sentman, M. F. Thomsen, H. R. Flindt, *Science* **188**, 459 (1975).
6. The detector complement of the University of Iowa Geiger tube telescope instrument comprises six miniature Geiger-Mueller tubes A, B, and C (EON Corporation type 6213) and D, E, and F (EON Corporation type 5107); and a single-element solid-state detector G (29 μm in thickness, totally depleted silicon). The single rates of A, B, C, D, and G and multiple coincidences AB, ABC, and DEF are transmitted. The directional detectors A, B, and G have conical physical collimators whose axes are perpendicular to the spin axis of the spacecraft. The spin axis is kept pointed at Earth to within about 1°. The spin period of the spacecraft was 7.693 seconds. During most of the encounter we obtained one 0.750-second sample of the counting rate of each of our ten detector channels at intervals of 8.25 seconds. A 360° angular distribution with nearly uniform spacing of samples was obtained each 115.5 seconds. Our instrument performed normally throughout the Saturn encounter and, because of the much lower counting rates than those in Jupiter's magnetosphere, only minor dead-time corrections were necessary for detectors A and B and none was necessary for the other detectors.

All positional data are taken from the post-encounter ephemeris [in ephemeris time (ET) at

- the spacecraft] prepared by the navigation section of the Jet Propulsion Laboratory (W. E. Kirhofer and W. H. Blume) and provided to investigators on 3 September. During the close-in portion of the trajectory the estimated accuracy of the radial distance from the spacecraft to the center of the planet is ± 60 km ($\pm 0.001 R_S$) and of planetocentric latitude is $\pm 0.02^\circ$ relative to the adopted polar axis of the planet $\lambda = 78.8142^\circ$, $\beta = 61.9324^\circ$ (ecliptic-equinox coordinates of 1950.0). The planetocentric longitude of the spacecraft is given for an adopted rotational period of 10 hours 14 minutes (sidereal) and an arbitrary prime meridian (that is, the hour angle of the vernal equinox of the planet measured from the adopted prime meridian of the planet was taken to be zero at 1950.0 ET). In this report, all times are Earth received times (ERT) [universal time (UT), referred to the Greenwich meridian] of the telemetry signal. At periapsis, $\text{ERT} = \text{ET} (\text{spacecraft}) - 50.2^{\text{sec}} + 86^{\text{min}} 20.5^{\text{sec}}$. The adopted unit of distance is the equatorial radius of the planet, $1 R_S = 60,000$ km.
7. J. H. Wolfe, J. D. Mihalov, H. R. Collard, D. D. McKibbin, L. A. Frank, D. S. Intriligator, *Science* **207**, 403 (1980).
 8. E. J. Smith, L. Davis, Jr., D. E. Jones, P. J. Coleman, Jr., D. S. Colburn, P. Dyal, C. P. Sonnett, *ibid.*, p. 407.
 9. M. H. Acuña and N. F. Ness, *ibid.*, p. 444.
 10. J. A. Simpson, T. S. Bastian, D. L. Chenette, G. A. Lentz, R. B. McKibbin, K. R. Pyle, A. J. Tuzzolino, *ibid.*, p. 411.
 11. W. Fillius, W. H. Ip, C. E. McIlwain, *ibid.*, p. 425.
 12. J. A. Van Allen and N. F. Ness, *J. Geophys. Res.* **74**, 71 (1969).
 13. T. Gehrels *et al.*, *Science* **207**, 437 (1980).
 14. J. W. Fountain and S. M. Larson, *Icarus* **36**, 92 (1978).
 15. K. Aksnes and F. A. Franklin, *ibid.*, p. 107.
 16. A. P. Ingersoll, G. S. Orton, G. Neugebauer, G. Münch, S. C. Chase, *Science* **207**, 439 (1980).
 17. W. A. Feibelman, *Nature (London)* **214**, 793 (1967).
 18. M. F. Thomsen and J. A. Van Allen, *Geophys. Res. Lett.* **6**, 893 (1979).
 19. A. L. Schardt, private communication.
 20. J. H. Trainor, F. B. McDonald, A. W. Schardt, *Science* **207**, 421 (1980).
 21. This work was supported in large part by Ames Research Center/NASA contract NAS2-6553 and the U.S. Office of Naval Research. We are indebted for assistance in many ways to C. F. Hall, R. P. Hogan, and R. O. Fimmel of the Ames Research Center; to R. L. Brechwald, D. D. Sentman (now at UCLA), R. F. Randall, D. E. Cramer, H. D. Owens, E. A. Freund, and E. D. Robison of the University of Iowa.

3 December 1979

Observations of Energetic Ions and Electrons in Saturn's Magnetosphere

Abstract. *The passage of Pioneer 11 by Saturn provided a detailed view of a planetary magnetosphere that is intermediate between those of Jupiter and Earth in both scale and the complexity of its dynamic processes. It appears to have at least three distinct regions: (i) an outer magnetosphere, extending from 17 to 7.5 Saturn radii, that resembles that of Earth in many important aspects; (ii) a slot region, between 7.5 and 4 Saturn radii, where a marked decrease in all protons and low-energy electrons is observed; and (iii) an inner region, extending from 4 Saturn radii to the ring edge, that features a sharp increase in the proton flux extending to energies greater than 20 million electron volts. A cutoff of both proton and electron fluxes occurred just beyond the nominal edge of the A ring.*

Data from the cosmic-ray experiment conducted by the Goddard Space Flight Center and the University of New Hampshire during the recent Pioneer 11 flyby of Saturn reveal a complex but moderately sized magnetosphere in which the planetary moons, rings, and temporal effects play key roles. This re-

port summarizes our first direct observations of the magnetosphere of this giant planet. The experiment provides detailed proton energy spectra and angular distributions from 0.2 to 22 MeV and electron energy spectra and angular distributions from 0.1 to 2 MeV. In addition, helium nuclei are measured in several intervals

between 0.65 and 22 MeV per nucleon (1). The spacecraft approached the Saturn system near the subsolar point and exited toward the dawn meridian (2). An overview of the energetic particle data is provided by the proton and electron time histories for three different energies of each component (Figs. 1 and 2). This limited spatial survey suggests a tentative division into three distinct regions:

1) Outer magnetosphere [magnetopause to 7.5 Saturn radii (R_S)]: this region is characterized by monotonically increasing fluxes and hardening of the spectra inward from the magnetopause. There are large and unusual changes in the angular distributions of low-energy electrons.

2) Slot region (7.5 to 4 R_S): the proton flux decreases by a factor of 50 and the low-energy electron flux by a factor of at least 10. The Saturn moons Dione, Tethys, and Enceladus, which orbit this region, appear to play major roles in reducing the fluxes.

3) Inner magnetosphere (4 R_S to nominal A ring edge): the proton fluxes increase rapidly inside the orbit of Enceladus, with deep flux depressions observed near the orbits of Mimas, Janus, and possibly S 11. The rapid proton increase extends to energies greater than 20 MeV and the proton energy spectra become complex. A sharp cutoff of all trapped particles was observed at the ring edge.

Prior to the encounter, no measurable fluxes of energetic ions or electrons were detected that could be attributed to Saturn. Thus there is no indication that Saturn's magnetosphere is a source of interplanetary electrons, as is Jupiter's (3, 4). A moderately sized solar cosmic-ray event was in progress during the encounter period, and fluxes of 10- to 20-MeV protons were detected in the outer magnetosphere. It is plausible that these were of solar cosmic-ray origin and had access to the magnetosphere via a Saturn tail region in the same manner that low-energy solar cosmic rays penetrate deep into Earth's magnetosphere (5). Studies are being carried out to determine how well the Saturn tail region can be defined by these observations.

In the following discussion, the three regions of the Saturn magnetosphere are described in greater detail.

Outer region. The time histories for 0.2-, 0.7-, and 1.2-MeV protons and 0.1-, 0.8-, and 1.1-MeV electrons in the outer region are shown in Figs. 1 and 2. The magnetopause was first encountered in the subsolar region at 17.3 R_S and is an effective boundary for particles of low rigidity (0.2-MeV protons and 0.5-MeV

electrons). A flux increase of about an order of magnitude was observed within $1 R_S$ of the boundary. Inside the magnetosphere, particle fluxes increase to a maximum at $7 R_S$, with a systematic hardening of both proton and electron spectra. The differential spectra can be represented by $j(E) \propto E^{-\gamma}$, where E is the kinetic energy of the particles. The spectral index γ for protons changes from 5.8 at $14 R_S$ to 4.1 at $7 R_S$. Superimposed on this steep spectrum is a hard component observable above ~ 2 MeV with $\gamma = 2$. It decreases in relative importance and loses statistical significance inside $10 R_S$. The spectral index and radial behavior of the higher energy proton component in

the outer region suggest that this component is of solar origin.

For both protons and electrons, there are departures from the monotonic flux increase with decreasing radial distance. These changes are particularly noticeable in the low-energy channels (Figs. 1 and 2) and are more pronounced in the dawn direction (outbound pass). Variations in solar wind conditions are probably the primary cause.

Further information about the outer region can be obtained by studying the angular distributions of the protons and electrons. For this type of study, counting rates are divided into eight 45° sectors for three proton channels from 0.5 to

2.2 MeV and for four electron channels from 0.1 to 2 MeV. The detection system scans in a plane that is perpendicular to the spin axis of the spacecraft, which in turn points at Earth. This geometry determines which physical effects (such as corotation, field-aligned streaming, and so forth) can be observed. In the analysis procedure, the particle distribution $J(\theta)$ is expressed as a Fourier series $J(\theta) = \sum_{n=0} A_n \cos n(\theta - \theta_n)$. First-order anisotropies (that is, A_1/A_0) can be produced by field-aligned streaming, corotation, or the effects of intensity gradients. No significant first-order anisotropies were observed for electrons. Significant A_1/A_0 values were measured

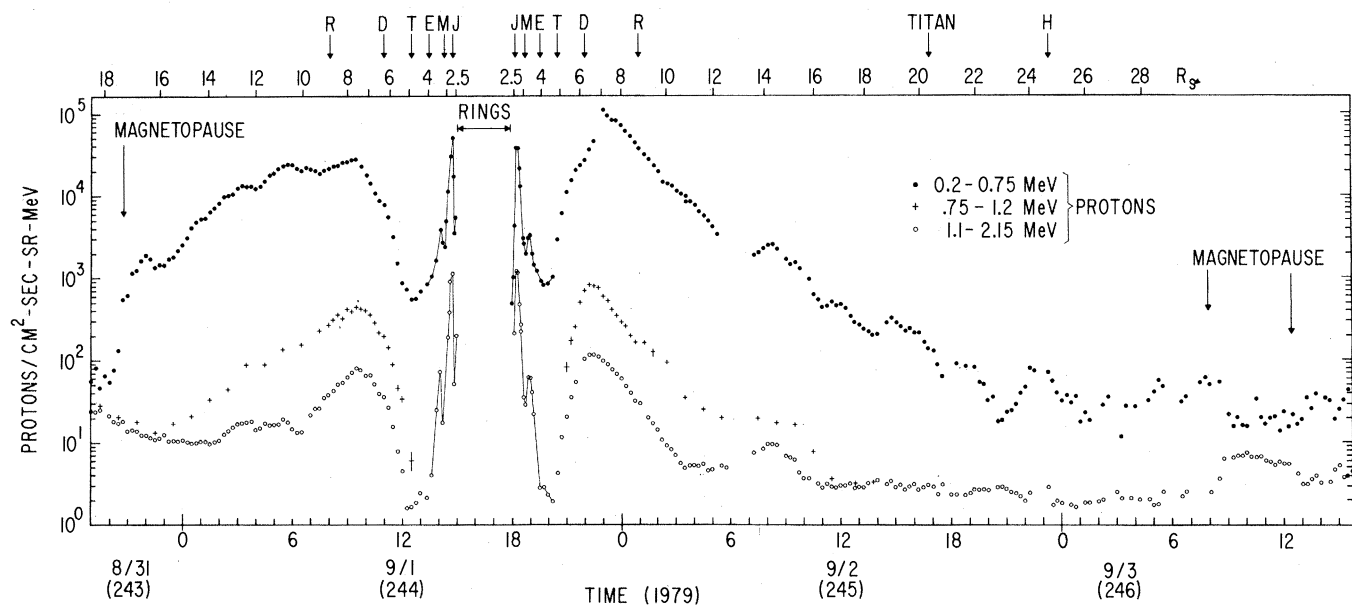


Fig. 1. Proton fluxes during the inbound and outbound passes of Pioneer 11. Arrows indicate the position of Rhea (*R*), Dione (*D*), Tethys (*T*), Enceladus (*E*), Mimas (*M*), Janus (*J*), Titan, and Hyperion (*H*). The object J 11 is located near the orbit of Janus.

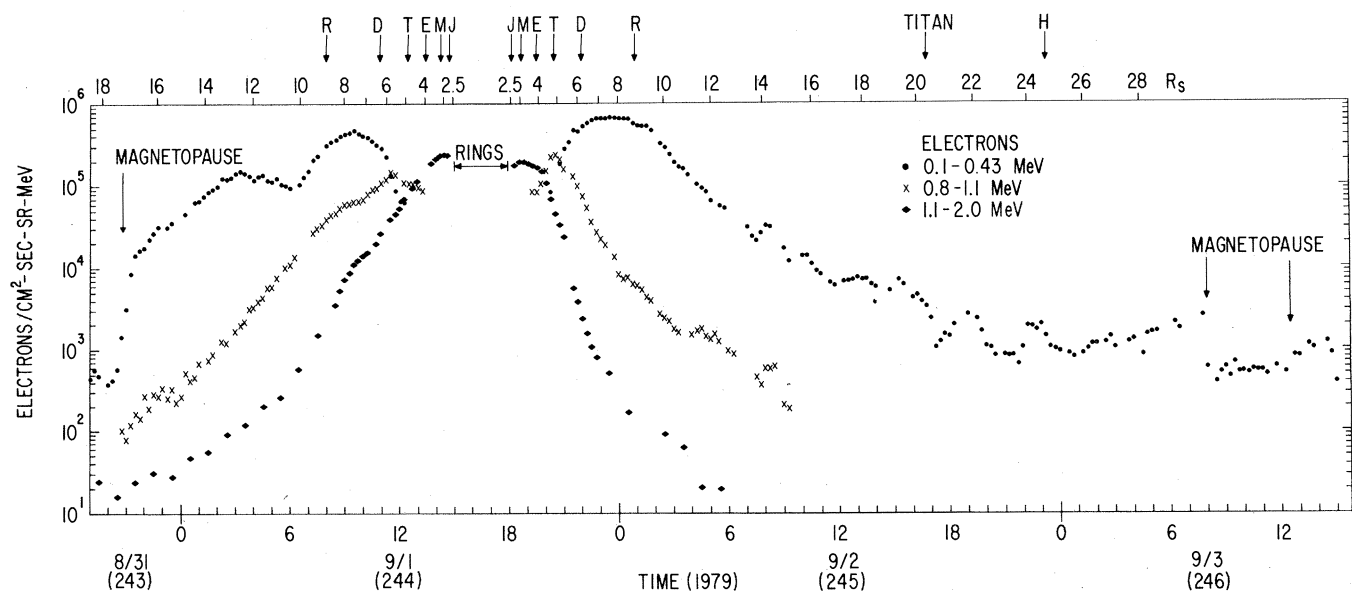


Fig. 2. Electron fluxes observed with Pioneer 11. Saturn satellites are abbreviated as in Fig. 1.

for the 0.5- to 2.2-MeV protons in the expected corotation direction. The corotation anisotropy is produced when the observer moves relative to the appropriate rest frame, which can be either the magnetospheric plasma or the magnetic field. The observed particles then have different energies and directions than in the rest frame, producing an anisotropy. The first-order anisotropy is given by the Compton-Getting effect (6) plus smaller corrections for the flux gradient and the "pancake" angular distribution. At 10.8 R_S , A_1/A_0 is 16.6 ± 3.1 percent, leading to a rotation velocity of 112 ± 36 km/sec, a fortuitously close agreement with the velocity of 110 km/sec expected from the period (10 hours 14 minutes) of Saturn's atmospheric markings (7).

Because of the symmetry of particle trajectories around magnetic field lines, the second-order anisotropy is either field-aligned, giving rise to "dumbbell" distributions, or perpendicular to the field direction, resulting in pancake distributions. Pancake distributions are generally found in Earth's magnetosphere for particles that have been trapped for a long time. The dumbbell distributions generally represent freshly injected particles or a situation in which particles with mirror points near the equatorial plane have been selectively removed by such a process as absorption by one of the planetary moons or other material. Dumbbell distributions can also result from shell splitting (8).

The second-order anisotropies of both electrons and protons are relatively

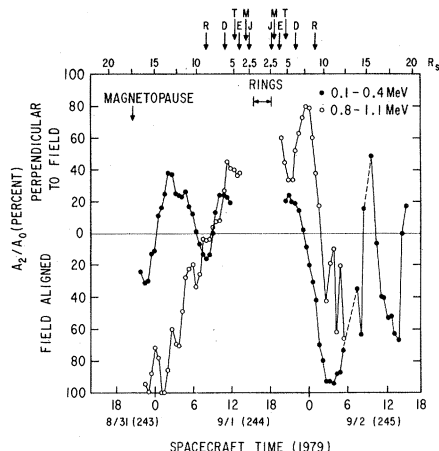
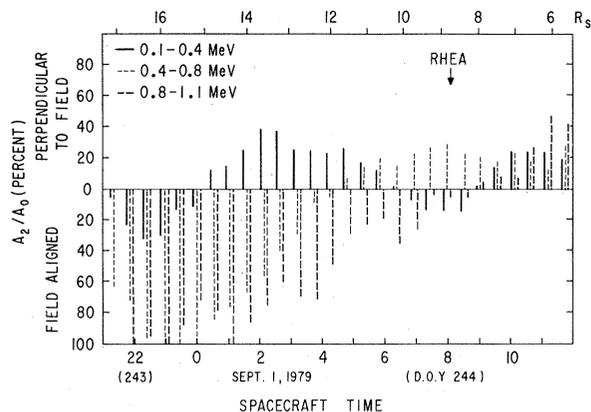


Fig. 3. Second-order anisotropy of 0.1- to 0.4-MeV and 0.8- to 1.1-MeV electrons (32-minute averages). The pitch-angle distributions perpendicular to the field correspond to $1 + b \sin^2\phi$, and field-aligned distributions correspond to $1 + b \cos^2\phi$, with $b = 2(A_2/A_0)(1 - A_2/A_0)^{-1}$. No corrections have been made for the inclination of the magnetic field relative to the scan plane. Saturn satellites are abbreviated as in Fig. 1.

25 JANUARY 1980

Fig. 4. Second-order anisotropies during the inbound pass of Pioneer 11. Averages of 32 minutes are shown for the three energy channels. Strongly energy-dependent distributions are observed between 15 and 8 R_S .



large. Figure 3 shows values of A_2/A_0 for two electron energies, with dumbbell values plotted down from isotropy and pancake values plotted up from isotropy ($A_2/A_0 = 0$). Near the magnetopause, all electron channels (0.1 to 2 MeV) have large dumbbell anisotropies. At 15 R_S , the 0.1- to 0.4-MeV electron distributions approach isotropy and then become distinctly pancake-shaped between 10 and 15 R_S . This channel again shows a dumbbell distribution between 10 and 8 R_S . The high-energy electrons (Fig. 3) also start with a dumbbell distribution near the magnetopause and progress first toward isotropy near 8 R_S and then increasingly toward a pancake distribution. This channel is typical of the trend of angular distributions at other energies, all of which start as dumbbell distributions and end as pancake distributions at 5 R_S . Such a change in the distributions is qualitatively consistent with inward diffusion, which selectively increases the velocity component perpendicular to the magnetic field, thus concentrating the particles near the equator into a pancake distribution. The same general trend is also evident during the outbound pass.

The behavior of the electron channel of lowest energy is clearly anomalous and asymmetrical with respect to the outbound pass. This asymmetry, when considered together with changes in the proton distributions, appears to be temporal in nature (Fig. 4). Between 10 and 8 R_S , the 0.4- to 0.8-MeV electrons have a normal or pancake distribution, while the energy intervals on either side are field-aligned.

The angular distribution of protons is always pancake-shaped in Saturn's outer magnetosphere. There is one period, around 10 R_S , when A_2/A_0 decreases to 20 percent from its average value of ~ 70 percent. This is exactly the time when the low-energy electron distribution changes directions. Both the low-energy electron and proton fluxes (Figs. 1 and 2)

show small decreases at the same time. These changes are observed just outside the orbit of Rhea on the inbound pass and inside during the outbound pass, so it is likely that they are mainly temporal variations and not absorption features.

Slot region. The proton flux at energies between 0.2 and 2.2 MeV is reduced by a factor of about 50 inside 7.5 R_S for a distance of $< 2 R_S$. At the same time, the angular distribution evolves from a normal pancake distribution to one that is isotropic. However, the spectral index γ is almost constant, varying only between 3.8 and 4.1. Above 0.5 MeV, the proton intensity in the slot region was actually less than the interplanetary value at the time Pioneer 11 entered the magnetosheath region.

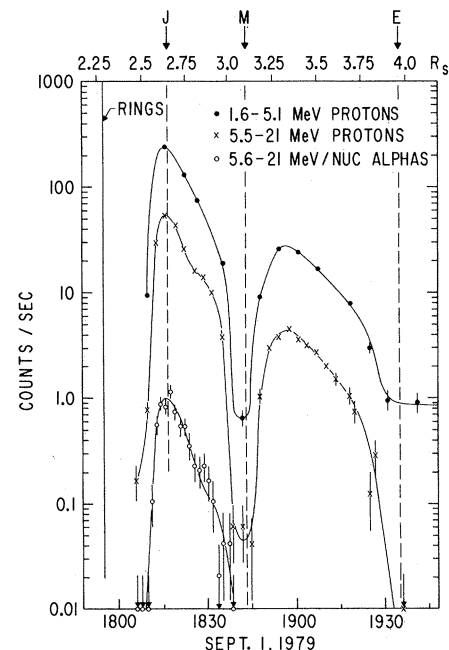


Fig. 5. Proton and alpha-particle fluxes in the inner magnetosphere during the outbound pass. The nominal orbits of Janus (J), Mimas (M), and Enceladus (E) are indicated by dashed lines. (Data for the inner region must be regarded as preliminary, since several important corrections have not been made.)

423

The decrease of low-energy electrons (Fig. 2) closely follows that of the protons both inbound and outbound. However, as the electron energy increases, the maxima and minima move closer to Saturn and become less distinct, until no dip is discernible in the 1.1-MeV channel. Thus the electron differential energy spectrum develops to a maximum between 0.1 and 1.1 MeV, and the maximum occurs at progressively higher energies as Saturn is approached. The shape of the electron spectrum inside $5 R_S$ is such that the detector response to bremsstrahlung in the shielding is probably the dominant contributor to the counts in the low-energy electron channels. (These channels are not plotted in Fig. 2 in the region where the electron intensities become uncertain.)

If the slot region is produced by the sweep-up effect of the satellites Dione, Tethys, and Enceladus, then the difference in electron response with energy can be understood in terms of differences in drift speed (9). Near-equatorial electrons with energies of 0.89, 1.07, and 1.22 MeV are in resonance with these moons and are minimally affected. In contrast, protons and low-energy electrons would be removed much more effectively. Such a mechanism would require symmetry between the inbound and outbound passes. The rise and decay of the 1.1-MeV proton flux (Fig. 1) was well defined. Extrapolating from these curves, we find an intersection at $6.5 R_S$ for the inbound pass and $6.35 R_S$ for the outbound pass. Dione is located at $6.3 R_S$. The proton flux starts to increase again just within the orbit of Enceladus.

The boundary between the outer magnetosphere and the slot region—that is, the intensity maximum of protons and low-energy electrons—is not as sharp. Furthermore, the positions of the maxima and of the peaks in the differential electron energy spectra are about 0.4 to $0.6 R_S$ closer to the planet on the outbound pass than on the inbound. This asymmetry may indicate that other processes besides absorption are significant in this region.

Inner region. Inside the orbit of Enceladus, the proton fluxes increase at all proton energies from 0.2 to above 20 MeV. The angular distributions are dumbbell-shaped, and well-defined absorption features coincide with the orbit of Mimas but not that of Janus (Fig. 5). Important corrections for dead-time effects, penetrating particles, helium nuclei, and electrons have still to be applied. These corrections could significantly alter the data shown in Fig. 5.

(The proton energy spectrum in this region is still under study.) Below 2 MeV, the spectral shape is $\propto E^{-3.4}$, but it is much flatter above 2 MeV. The 1- to 2-MeV electron flux approaches a plateau region as a function of radius, with no major absorption features.

An important clue to the origin of the particles in the inner region is provided by the presence or absence of heavier nuclei. A preliminary analysis of our data indicates an upper limit for the He/H ratio of 0.01 for 10 to 20 MeV per nucleon (Fig. 5). At lower energies, this ratio appears to increase to ~ 0.1 .

Several well-known mechanisms appear to be responsible for the observed phenomenology. At the particle energies examined in this experiment, Saturn's outer magnetosphere resembles that of Earth. Below 2 MeV, the flux increase and energy spectra are those that would be expected if particles were injected near the magnetopause and then further accelerated by inward radial diffusion with conservation of the first and second adiabatic invariants. The strange behavior of the electron angular distributions (Figs. 3 and 4) indicates that resonant wave-particle interactions probably occur, presumably with waves generated in the magnetosphere. More detailed analysis of the shape of the angular distributions revealed deep notches in the distributions of 1-MeV electrons, perpendicular to the magnetic field at $12 R_S$ inbound and field-aligned at $8 R_S$ outbound. These interactions are probably the cause for the difference in behavior of the second harmonic between the inbound and outbound passes (Fig. 3).

The direction of both the magnetic field and the trapped particle anisotropies during the outbound pass indicates that the magnetosphere is distended, possibly into a shape approaching that of a tail or plasma disk. Magnetospheric plasma was shown to be present between 4 and $7 R_S$ (10), and it may be considerably more extensive.

Dione, Tethys, and Enceladus appear to play major roles in establishing the slot region. However, the gyroradius of a 1-MeV proton is 3.5 times the radius of Dione. For both Tethys and Enceladus, this gyroradius is comparable to the satellite radii. If the particle diffusion coefficient is large, then other processes may be involved. These might include the effects of additional, as yet unobserved material orbiting Saturn in the slot region, or interactions with the ambient plasma (10). The latter process could also explain the observed asymmetry between the inbound and outbound passes.

The inner magnetosphere may be very

stable. Mimas appears to be effective in removing energetic protons; still, its radius (270 km) is not much larger than the 196-km gyroradius of 1-MeV protons. No comparable absorption feature was observed at the nominal orbit of Janus ($2.65 R_S$), even though the ratio between proton gyroradius and satellite radius is only 10 percent smaller than for Mimas. We consider this strong evidence that Janus orbits inside $2.59 R_S$ or is much smaller than its nominal 150-km radius. A mean orbital position of $2.52 \pm 0.04 R_S$ corresponds to the center of the absorption slot observed during the inbound pass. A critical reexamination of astronomical data by Aksnes and Franklin (11) showed that the orbit of Janus cannot be determined definitively from available data. They found two orbits (2.5222 and $2.5242 R_S$) that are consistent with most of the observations, but have somewhat larger residuals. Data points for the present experiment were not taken often enough to determine whether other objects, such as J-11, contributed to this absorption feature.

If diffusion times are slow enough to permit effective sweep-out by a small satellite like Mimas, then the long lifetime of particles between satellite orbits would permit the buildup of a substantial particle population even from a relatively weak source such as cosmic-ray albedo neutrons. Therefore, the two obvious sources for these particles in the inner zone are (i) the inward diffusion of solar wind particles energized in the outer region and (ii) protons from the decay of secondary neutrons that were produced by primary cosmic rays incident on the surface of Saturn and the ring material. The dumbbell angular distribution is consistent with both processes. In fact, both processes are expected to contribute to the population of energetic particles. The apparent presence of helium nuclei indicates that particles of solar wind origin represent an important component up to energies of at least 20 meV per nucleon.

J. H. TRAINOR
F. B. McDONALD
A. W. SCHARDT

NASA/Goddard Space Flight Center,
Greenbelt, Maryland 20771

References and Notes

1. J. H. Trainor, F. B. McDonald, B. J. Teegarden, W. R. Webber, E. C. Roelof, *J. Geophys. Res.* **79**, 3600 (1974).
2. J. W. Dyer, *Science* **207**, 400 (1980).
3. B. J. Teegarden, F. B. McDonald, J. H. Trainor, W. R. Webber, E. C. Roelof, *J. Geophys. Res.* **79**, 3615 (1974).
4. T. F. Conlon, *ibid.* **83**, 541 (1978).
5. M. Schuler, *Space Sci. Rev.* **17**, 3 (1975).
6. M. A. Forman, *Planet. Space Sci.* **18**, 25 (1970).
7. C. W. Allen, *Astrophysical Quantities* (Humanities, Atlantic Highlands, N.J., 1973).

8. J. G. Roederer, *Rev. Geophys. Space Phys.* **10**, 599 (1972).
9. A. Mogro-Campero and R. W. Fillius, *J. Geophys. Res.* **81**, 1289 (1976).
10. See J. H. Wolfe, J. D. Mihalov, H. R. Collard, D. D. McKibbin, L. A. Frank, and D. S. Intrilligator [*Science* **207**, 403 (1980)] for plasma results during encounter.
11. K. Aksnes and F. A. Franklin, *Icarus* **36**, 107 (1978).
12. We thank R. Finnel, C. Hall, J. Wolfe, and especially R. Hogan for their attention and assistance in carrying out the successful Pioneer 11

mission. Discussions with T. G. Northrop concerning interpretation of the data are gratefully acknowledged. Our programming and data-processing team of N. Lal, H. Domchick, and J. Broomhall did an outstanding job of processing the encounter data in near real time. We also thank E. J. Smith and coinvestigators for supplying the magnetic field data from the helium vector magnetometer and M. Acuna and N. Ness for data from the high-field, flux-gate magnetometer.

3 December 1979

Trapped Radiation Belts of Saturn: First Look

Abstract. *Pioneer 11 has made the first exploration of the magnetosphere and trapped radiation belts of Saturn. Saturn's magnetosphere is intermediate in size between Earth's and Jupiter's, with trapped particle intensities comparable to Earth's. The outer region of Saturn's magnetosphere contains lower energy radiation and is variable with time; the inner region contains higher energy particles. The pitch angle distributions show a remarkable variety of field-aligned and locally mirroring configurations. The moons and especially the rings of Saturn are effective absorbers of trapped particles; underneath the rings, the trapped radiation is completely absorbed. We confirm the discovery of a new ring, called the F ring, a new division, the Pioneer division, and a moon, called 1979 S 2. The latter has probably been seen from Earth. There may be evidence for more bodies like 1979 S 2, but at this stage the interpretation of the data is ambiguous. Using particle diffusion rates, we estimate that the cross-sectional area of the F ring is $> 7 \times 10^{13}$ square centimeters and that the opacity is $> 10^{-5}$. Cosmic-ray albedo neutron decay should be looked into as a source of energetic particles in the inner magnetosphere of Saturn.*

On its historic flight past Saturn, Pioneer 11 carried instrumentation for the measurement of magnetospheric particles and fields. One of these instruments was a trapped radiation detector package designed and built at the University of California, San Diego (UCSD) (Table 1). Data obtained with this package are providing (i) confirmation of the existence of a magnetosphere and trapped radiation belt at Saturn, (ii) greater understanding of that magnetosphere and measurements of trapped particle fluxes and energies, (iii) the opportunity to investigate particle acceleration processes under new conditions and to compare them with activity in other magnetospheres, and (iv) information about ring and satellite absorption effects, including the wake of what is probably a previously undiscovered object.

Traveling to Saturn by way of Earth and Jupiter, Pioneer 11 crossed three magnetospheres and, with its sister spacecraft Pioneer 10, gathered excellent material for comparative studies. Figure 1 shows the intensities and radial extents of particles in a common energy range at the three planets. Other comparative features that can be seen include the effects of moons and rings and the modulation of the radiation levels by planetary rotation.

Earth's moon is well outside the terrestrial magnetosphere and has no effect on it. However, many of the moons of

Jupiter and Saturn are inside the zone of trapped radiation and interact strongly with the trapped particles. In Fig. 1, the arrows at the orbits of Io and Amalthea point to dips caused by absorption of the radiation. There are analogous absorption features at Saturn, too, but they are not shown distinctly in Fig. 1. The ring of Jupiter (*I*) produces an absorption dip

Fig. 1. Magnetospheres of three planets. These profiles of the radiation belts of Earth, Jupiter, and Saturn were made by University of California instrumentation on two Pioneer spacecraft. The profile of Earth's radiation belt was made in the dawn sector by Pioneer 10; those of Jupiter and Saturn were made by identical instrumentation on Pioneer 11 outbound in the noon and dawn sectors, respectively. The data shown are from an electron scatter detector with a geometric factor of $1.04 \times 10^3 \text{ cm}^2 \text{ sr}^{-1}$ for electrons $> 0.255 \text{ MeV}$. In the Jupiter magnetosphere inside Io, this detector responded mainly to omnidirectional electrons penetrating the shielding. For these particles the energy threshold is 35 MeV and the geometric factor 0.038 cm^2 . Note that the abscissa is in kilometers. To normalize to planetary radii, divide by 6371 km for Earth, 71,372 km for Jupiter, and 60,000 km for Saturn.

like that of the moons (2), but the rings of Saturn produce the most dramatic effect of all. The trapped radiation is completely absorbed at the outer edge of the A ring and, on lines of force intercepted by the Saturn rings, cosmic rays fall to less than one fifth of their interplanetary level. Our counting rates here were the lowest recorded in the entire flight.

Modulation at the planetary rotation rate is visible only at Jupiter, where the gross intensity variations outside the orbit of Io carry the 10-hour period of Jupiter's rotation. Earth's magnetosphere could produce a 24-hour modulation if an observatory could be held stationary at a chosen location. However, the near-Earth data shown here span only 1 hour, so there is no chance of seeing such an effect. Like Jupiter, Saturn has a rotation period of 10 hours, but if modulation occurs at this frequency, it is not readily apparent. It is natural to attribute this uniqueness to the remarkable symmetry of Saturn's magnetic field, which has a dipole moment with near-zero values for both tilt and offset (3).

Figure 2, A to C, shows a time profile (4) of Saturn's magnetosphere as seen by several channels of the UCSD instrument. Refer to Fig. 3 for the encounter geometry and Table 1 for a description of the detectors.

The outer region of Saturn's magnetosphere extends from ~ 6 Saturn radii (R_S) (5-7) to the magnetopause. It is strongly influenced by the time-variable solar wind, and it contains particles of lower energy than the inner region. Pio-

